Dark current analysis of Si homojunction interfacial work function internal photoemission far-infrared detectors

H. X. Yuan and A. G. U. Perera[a)]
Department of Physics and Astronomy, Georgia State University, Atlanta, Georgia 30303

(Received 7 November 1994; accepted for publication 6 February 1995)

A detailed theoretical investigation of dark current mechanisms is performed for a novel Si n^+-i homojunction interfacial work function internal photoemission (HIWIP) far-infrared (FIR) detector. Thermionic emission, thermionic field emission and field emission currents, including the image force effect, are calculated and compared as functions of bias voltage and temperature. The bias and temperature dependence of detector noise equivalent power (NEP), limited by thermal noise and background noise, is also calculated. From these results, the optimal operating temperatures and bias voltages are determined. Results show that Si HIWIP FIR detectors may have a performance comparable to the conventional Ge FIR detectors, with some unique advantages over them. © *1995 American Institute of Physics.*

Several Si homojunction infrared detector concepts based on internal photoemission were proposed and demonstrated recently.[1–5] The basic detector structure is characterized by an interfacial work function (or barrier) existing between a heavily doped absorber/emitter layer and a lightly doped (or intrinsic) layer. The interfacial barrier height (Δ), which defines the detector cutoff wavelength, λ_c (μm)$=1.24/\Delta$ (eV), is a function of device parameters and applied voltage. In a recent paper,[6] we have distinguished three types of homojunction internal photoemission detectors according to the emitter layer doping concentration (N_e), and shown that the type II detector (which is defined as N_e being above the Mott transition value but below the value at which $\Delta=0$, and here is labeled as homojunction interfacial work function internal photoemission (HIWIP) detector) can have a high performance for far-infrared (FIR) detection with a tailorable λ_c. Present FIR detectors used or under development for the 40-220 μm range are extrinsic Ge photoconductors (unstressed or stressed)[7] and Ge blocked-impurity-band (BIB) detectors.[8] Similar to Ge BIB detectors, Si HIWIP FIR detectors can avoid most of the shortcomings of conventional Ge photoconductors. Although the quantum efficiency (η) of the Si HIWIP detector is limited by the internal photoemission mechanism, the material advantages essentially will lead to excellent performance for large scale focal plane arrays.[9]

So far, the HIWIP detector concept has been demonstrated only for forward biased commercial p-i-n and p-i devices at low temperatures, with λ_c's as long as 220 μm for Si[3] and very low dark currents.[1,5] Since these devices were not designed for infrared detection, detector performance was not optimized. In order to fabricate detectors and obtain high performance, better understanding of various physical mechanisms limiting detector performance is essential, requiring detailed modeling work. In our recent paper,[6] the photoresponse performance of type II HIWIP detectors was analyzed in detail. The relationship between Δ (or λ_c) and N_e was derived and calculated. An analytic model was introduced to calculate η. In this letter, the dark current mechanisms of the HIWIP detector are investigated in detail, and the ultimate detector performance, limited by thermal or background noise, is calculated.

The proposed structure for a frontside illuminated single layer n^+-i HIWIP detector is shown in Fig. 1(a), on which an external bias is applied. The structure consists of the emitter, intrinsic, and collector layers, with the respective thicknesses represented by W_e, W_i, and W_c. The top contact layer is formed as a ring surrounding the active area to minimize absorption loss. The collector layer is moderately doped, so that even at low temperatures it has a relatively low resistivity due to the impurity band conduction, while it is still transparent in the FIR range when the photon energy is smaller than the impurity ionization energy.

The energy band diagram of the detector structure is shown in Fig. 1(b), where the image force effect causes a lowering ($\Delta\phi$) of the interfacial barrier height. The interfacial work function is given by $\Delta=\Delta E_c-E_F-\Delta\phi$, where ΔE_c is the conduction band edge offset due to the band gap narrowing in the heavily doped emitter layer and E_F the Fermi energy. By using an expression derived from the high density theory,[10] the zero field work function dependence on the emitter layer doping concentration (N_e) has been calculated.[6] Since Δ can become arbitrary small by increasing N_e, theoretically, there is no restriction on λ_c, which is tailorable in the FIR range. The barrier lowering and the barrier maximum position are given by[11] $\Delta\phi=\sqrt{qF/4\pi\epsilon_0\epsilon_s}$ and $x_m=\sqrt{q/16\pi\epsilon_0\epsilon_s F}$, respectively, where $F=V_b/W_i$ is the electric field in the i-region and V_b

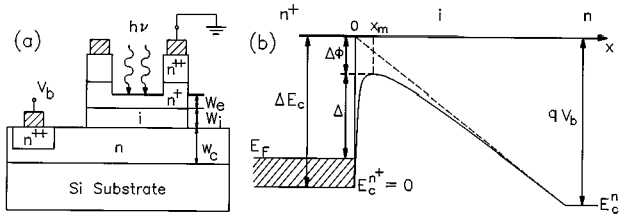

FIG. 1. (a) Basic structure used in the calculation and (b) energy band diagram of frontside illuminated n^+-i HIWIP FIR detector.

[a)]Electronic mail: phyuup@gsusgi1.gsu.edu

 0003-6951/95/66(17)/2262/3/$6.00

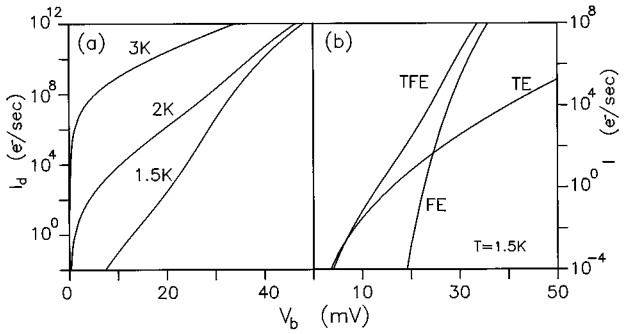

FIG. 2. Dark current-voltage characteristics: (a) results at different temperatures, and (b) comparison of thermionic emission (TE), thermionic field emission (TFE) and field emission (FE) current components at $T=1.5$ K.

the applied voltage. Thus, λ_c can also be controlled to a certain extent by the bias voltage.

Under illumination, the emitter layer absorbs the incident photons mainly through free carrier absorption mechanism. Some of the photoexcited electrons can escape over the interfacial barrier, and reach the collector layer. The total η is determined by photoexcitation, emission to the interfacial barrier, hot electron transport, and barrier collection due to the image force effect. In order to get high internal quantum efficiency, the emitter layer thickness should be thin enough, in spite of the reduction of the photon absorption efficiency. Thus, the optimal thickness is a tradeoff of photon absorption and hot electron scattering, as calculated in our recent paper.[6] In addition, η will increase with the electric field due to the enhancement of the barrier collection probability.

In the dark condition, an electron may transport across the barrier either by thermal process, or tunneling process, or a combination of both, depending on the energy location (E) of the electron. The process will be thermionic emission (TE) for $E>\Delta+E_F$, thermionic field emission (TFE) or thermally assisted tunneling for $E_F<E<\Delta+E_F$, and field emission (FE) or direct tunneling for $0<E<E_F$. The TE current density is given by the Richardson-Dushmann equation: $J_{TE}=A^{**}T^2\exp(-\Delta/k_BT)$, where $A^{**}=f_pA^*$, $A^*=4\pi qm^*k_B^2/h^3=120(m^*/m_0)$ A cm^{-2} K^{-2} is the Richardson constant, f_p the barrier escape probability, and m^* the effective electron mass. For n-type Si, $m^*\approx 2.1m_0$.[11] f_p is determined by the electron-phonon scattering in the image force potential well. As a first approximation, f_p is given by[11] $f_p=\exp(-x_m/L_s)$, where L_s is the scattering length. Due to f_p, the TE current is voltage dependent, especially in the low voltage range.

The tunneling current density flowing through the barrier, which includes both TFE and FE, is given by

$$J_t=J_{\rm TFE}+J_{\rm FE}=\frac{qm^*}{2\pi^2\hbar^3}\int f(E)T_t(E,E_\perp)dEdE_\perp, \qquad (1)$$

where $f(E)=\{1+\exp[(E-E_F)/k_BT]\}^{-1}$ is the Fermi-Dirac distribution function, T_t the tunneling probability, E the total energy of the electron, and $E_\perp$ the energy associated with the momentum perpendicular to the direction of tunneling (or transverse momentum, which in effect reduces the tunneling probability). T_t can be calculated using the WKB approximation, given by

$$T_t(E,E_\perp)=\exp\left(-2\int_{x_1}^{x_2}|k_x|dx\right), \qquad (2)$$

where $|k_x|=\sqrt{(2m_t/\hbar^2)(U-E_\perp+E)}$ is the wave vector in the tunneling direction, $U=\Delta E_c-qFx-q/16\pi\epsilon_0\epsilon_s x$ the potential energy, and m_t the tunneling effective mass component. For Si, $m_t=0.26m_0$. In Eq. (2), x_1 and x_2 are the classical turning points, given by $x_{1,2}=(E_1/2qF)\times[1\mp\sqrt{1-(q^3F/4\pi\epsilon_0\epsilon_sE_1^2)}]$, where $E_1=\Delta E_c-E_\perp+E$. The electron-phonon scattering in the image force potential well will further reduce T_t. Thus, the effective tunneling probability becomes $T_t^*=T_t\exp(-x_1/L_s)$.

In Eq. (1), the integration limits for $E_\perp$ are $0<E_\perp<\min(E-E_c^n,E)$, where $E_c^n=\Delta E_c-qV_b$ is the conduction band edge of the collector layer. The integration limits for E are $\max(E_F,E_c^n)<E<\Delta E_c-\Delta\phi$ for the TFE current J_{TFE}, and $\max(0,E_c^n)<E<E_F$ for the FE current J_{FE}. The total dark current is the sum of TE, TFE and FE currents, that is, $I_d=A_D(J_{\rm TE}+J_{\rm TFE}+J_{\rm FE})$, where A_D is the detector area. For photoemission detectors, the main noise mechanism is due to the shot noise.[12] The total noise current is contributed by the combination of the background photon noise and the thermal noise, given by $i_n=\sqrt{2q(I_B+I_d)}$ A/$\sqrt{\rm Hz}$, where $I_B=q\eta Q_BA_D$ is the background photocurrent and Q_B the background photon flux density.

The detector noise equivalent power is given by $\mathrm{NEP}_\lambda=i_n/R_\lambda$ W/$\sqrt{\rm Hz}$, where $R_\lambda=q\eta\lambda/hc$ is the responsivity (A/W). When the detector noise is dominated by the background photon noise, the detector has background limited performance (BLIP) with $\mathrm{NEP}_{\rm BLIP}=(hc/\lambda)\sqrt{(2Q_BA_D)/\eta}$ W/$\sqrt{\rm Hz}$. The BLIP temperature, $T_{\rm BLIP}$, is determined by the equation $I_B(\lambda,V_b)=I_d(V_b,T_{\rm BLIP})$.

Based on above equations and our previous work,[6] we have calculated the voltage and temperature dependence of dark current and NEP, for a Si n^+-i HIWIP detector with $N_e=3\times10^{19}$ cm^{-3} and the corresponding optimal $W_e=100$ Å. For this detector at $V_b=20$ mV, $\lambda_c=240$ μm, $\lambda_p=109$ μm (peak wavelength), and $\eta_p=6.6\%$ (peak quantum efficiency).[6] In the calculation, $W_i=0.5$ μm and $A_D=1\times10^{-3}$ cm^2 were used. Other parameters used are the same as in Ref. 6. It is expected that by using multilayer structures the effective η may be further increased due to the increased photon absorption efficiency and possible photocurrent gain enhancement.[5]

The dark current-voltage curves calculated at different temperatures are shown in Fig. 2(a). The comparison of TE, TFE and FE current components at $T=1.5$ K, is given in Fig. 2(b). At high temperatures TE current is dominant almost in the whole voltage range of interest. But at low temperatures and high voltages TFE current will exceed TE current. For example, at $T=1.5$ K, the detector is limited by TE current below $V_b=7$ mV and by TFE current at larger biases. In the bias range in Fig. 2(b), FE current is always smaller than TFE current even though it exceeds TE current at 25 mV. All

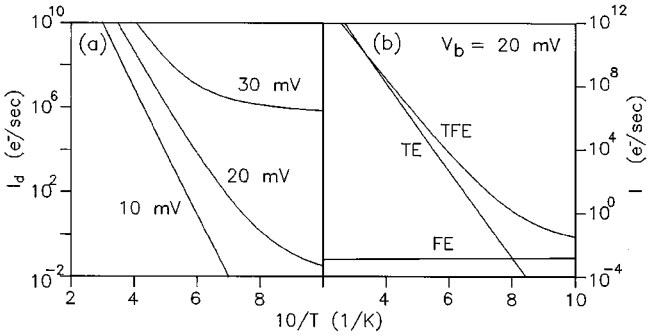

FIG. 3. Temperature dependence of dark current: (a) results at different biases, and (b) comparison of various current components at $V_b = 20$ mV.

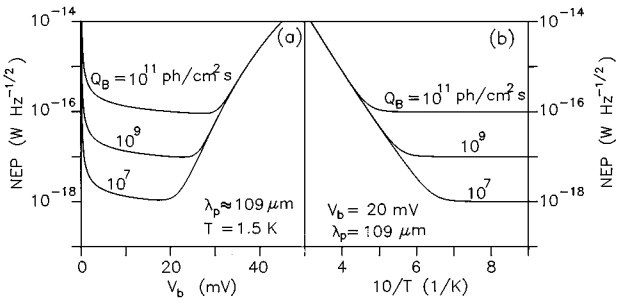

FIG. 4. NEP dependence on (a) bias and (b) temperature, calculated at $\lambda_p = 109\ \mu$m and under different backgrounds.

three components increase with increasing bias, among which the curve slope is largest for FE and smallest for TE.

Figure 3(a) shows the temperature dependence of dark current calculated at different biases. Comparison of the components at $V_b = 20$ mV is shown in Fig. 3(b). At lower biases, TE current dominates almost in the whole temperature range of interest, while at large biases, TFE current becomes dominant in the low temperature range. For example, at $V_b = 20$ mV, the detector is dominated by TE current above 3 K and by TFE current at lower temperatures. Among these current components, both TE and TFE decrease with decreasing temperature, and TE has the strongest temperature dependence. In contrast, FE is almost temperature insensitive, only increasing slightly with lowering temperature, which is due to the increase of the electron number below the Fermi level as temperature decreases. TFE current has a strong temperature dependence in the high temperature range, where it is limited by thermal process, and shows a weak temperature dependence in the low temperature range, where it is limited by tunneling. The transition temperature is around that point at which the TE curve intersects the FE curve, as shown in Fig. 3(b).

The voltage and temperature dependence of NEP calculated at $\lambda = 109\ \mu$m (which is the λ_p at $V_b = 20$ mV, corresponding to $\lambda_c = 240\ \mu$m) and with different background photon flux density (Q_B) are shown in Figs. 4(a) and 4(b), respectively. For a fixed temperature, NEP first decreases as the bias increases, where it is limited by background photon noise. Then it increases with a further increase in V_b, when limited by thermal noise. Therefore, an optimal bias voltage ($V_{\rm op}$) can be found from the minimum of NEP–V_b curve ($\mathrm{NEP}_{\rm min}$). Both $V_{\rm op}$ and $\mathrm{NEP}_{\rm min}$ decrease as Q_B reduces, which is due to the reduction of background noise. At $T = 1.5$ K and $Q_B = 10^7$ ph/cm² s, $V_{\rm op} = 18$ mV and $\mathrm{NEP}_{\rm min} = 1.1 \times 10^{-18}$ W/$\sqrt{\rm Hz}$. For a fixed V_b, NEP first decreases as temperature lowers, where it is limited by thermal noise. Then it no longer depends on T when limited by background noise, reaching the background limited value ($\mathrm{NEP}_{\rm BLIP}$). The transition temperature is just the background limited temperature ($T_{\rm BLIP}$). As Q_B decreases, both $T_{\rm BLIP}$ and $\mathrm{NEP}_{\rm BLIP}$ decrease. At $V_b = 20$ mV and $Q_B = 10^7$ ph/cm² s, $T_{\rm BLIP} = 1.3$ K and $\mathrm{NEP}_{\rm BLIP} = 1.0 \times 10^{-18}$ W/$\sqrt{\rm Hz}$.

In summary, we have calculated the dark current and NEP for the Si HIWIP FIR detector as functions of bias and temperature. Results show that TFE current dominates almost in the whole useful voltage and temperature ranges, and as N_e increases (hence longer λ_c), both optimal bias and $T_{\rm BLIP}$ decrease. The theoretical performance of HIWIP detectors, based on our present model, is comparable to that of conventional Ge FIR photoconductors. Together with its unique features, the Si HIWIP FIR detector can match or exceed the capability of Ge FIR detector.

This work was supported in part by the NSF under Grant No. ECS94-12248. The authors acknowledge Steven Matsik and Young-Jie Ko for their technical help.

[1] D. D. Coon, R. P. Devaty, A. G. U. Perera, and R. E. Sherriff, Appl. Phys. Lett. **55**, 1738 (1989).
[2] S. Tohyama, N. Teranishi, K. Konuma, M. Nishimura, K. Asai, and E. Oda, IEEE Trans. Electron Devices **ED-38**, 1136 (1991).
[3] A. G. U. Perera, R. E. Sherriff, M. H. Francombe, and R. P. Devaty, Appl. Phys. Lett. **60**, 3168 (1992).
[4] H. C. Liu, J.-P. Noel, Lujian Li, M. Buchanan, and J. G. Simmons, Appl. Phys. Lett. **60**, 3298 (1992).
[5] A. G. U. Perera, J.-W. Choe, M. H. Francombe, R. E. Sherriff, and R. P. Devaty, Superlattices Microstructures **14**, 123 (1993).
[6] A. G. U. Perera, H. X. Yuan, and M. H. Francombe, J. Appl. Phys. **77**, 915 (1995).
[7] E. E. Haller, Infrared Phys. **35**, 127 (1994).
[8] D. M. Watson, M. T. Guptill, J. E. Huffman, T. N. Krabach, S. N. Raines, and S. Satyapal, J. Appl. Phys. **74**, 4199 (1993).
[9] T. L. Lin and J. Maserjian, Appl. Phys. Lett. **57**, 1422 (1990).
[10] S. C. Jain and D. J. Roulston, Solid State Electron. **34**, 453 (1991).
[11] S. M. Sze, *Physics of Semiconductor Devices*, 2nd ed. (Wiley, New York, 1981), Chap. 5.
[12] R. J. Keyes, *Optical and Infrared Detectors*, Topics in Applied Physics Vol. 19 (Springer, Berlin, 1980), p. 41.